Remanent magnetization in CoO antiferromagnetic nanoparticles

N. J. O. Silva,* A. Millán, and F. Palacio
Instituto de Ciencia de Materiales de Aragón, CSIC-Universidad de Zaragoza, 50009 Zaragoza, Spain and Departamento de Física de la Materia Condensada, Facultad de Ciencias, Universidad de Zaragoza, 50009 Zaragoza, Spain

M. Martins and T. Trindade
Departamento de Química and CICECO, Universidade de Aveiro, 3810-193 Aveiro, Portugal

I. Puente-Orench and J. Campo
Instituto de Ciencia de Materiales de Aragón, CSIC-Universidad de Zaragoza, 50009 Zaragoza, Spain and Institut Laue-Langevin, BP 156, F-38042 Grenoble Cedex 9, France
(Received 18 May 2010; revised manuscript received 23 July 2010; published 20 September 2010)

We report a study on the remanent magnetization M_r induced by field cooling across the ordering temperature T_N in antiferromagnetic CoO nanoparticles with different sizes. The nanoparticles are composed by a structurally and magnetically ordered core and a structurally ordered and magnetically disordered shell with a thickness of about 2 nm. The ordered core has cell parameters, moments direction, and modulus similar to those of bulk CoO. M_r is shown to be proportional to the cooling field H_{cool}. The low-temperature saturation values of M_r $[M_r(0)]$ in the CoO nanoparticles are about two orders of magnitude higher than those found for bulk CoO. $M_r/M_r(0)$ of CoO nanoparticles scales with temperature in a single curve, independently on the magnitude of H_{cool} and on nanoparticles size, except for temperatures near to T_N since T_N is size dependent.

DOI: 10.1103/PhysRevB.82.094433 PACS number(s): 75.30.Cr, 75.50.Ee, 75.50.Tt

I. INTRODUCTION

It is known that bulk antiferromagnetic (AF) materials can exhibit remanent magnetization M_r. This is the case of 3*d* random-field AF (Ref. 1) and of AF compounds where magnetic sites are diluted with nonmagnetic impurities,[2] for instance. The origin of M_r in the former is spin readjustments within the domain walls of immobile AF domains (at low temperatures) being M_r also affected by domain growth at higher temperatures.[1] In AF materials diluted with nonmagnetic impurities, the saturation of M_r occurs at fields on the order of a few oersteds and the proposed mechanism is the pinning of domain walls due to the nonmagnetic impurities and lattice defects.[2]

Small nanoparticles (NPs) are expected to be monodomain and therefore the bulk mechanisms for the generation of M_r associated to domain walls are not effective. Alternatively, M_r can arise associated with uncompensated and canted moments due to surface and/or in-volume effects. In NPs, much attention has been paid to the interaction between AF and ferromagnetic components in the context of exchange bias (see, for instance the review in Ref. 3) but less to the existence of a M_r associated to the AF component,[4,5] although it was recognized that the M_r of the AF component and the associated uncompensated moments have an important role in the exchange bias phenomena.[4,6] In most of the cases, the largest fraction of M_r is given by a ferromagnetic/ferrimagnetic component, and the role of the AF component is to keep the moment in a fixed direction by increasing the coercivity and the blocking temperature of the NPs.[7] In a recent example, the AF component was also found to increase the ordering temperature of the ferrimagnetic component.[8]

Considering surface vs in-volume effects, most studies are devoted to ferrimagnetic nanoparticles, where unlike in AF NPs, surface is the origin of a reduction in the magnetic moment. These studies are not unanimous with some authors claiming the preferential surface canting[9,10] in disagreement with others where finite-size/in-volume effects are observed.[11,12] Studies comparing surfactant-coated particles with uncoated ones show that the magnetic properties are greatly affected by the surfactant-particle interaction, suggesting the surface nature of this phenomena.[13,14] Another attempt to characterize the origin of the uncompensated moment consists in comparing the particle size obtained from the electron microscopy or x-ray diffraction (XRD) techniques with the magnetic size derived from the field dependence of the magnetization, being the latter generally lower.[15]

In AF NPs, surface is often invoked as the origin of uncompensated moments.[5,16–18] Evidence for the surface origin includes the linear decreasing of the saturation magnetization with temperature.[16,19–21] The uncompensated moments include those arising from an odd number of AF planes, generation of vacancies and oxidation of surface atoms.[5] In studies where surface effects are highlighted, the nanoparticles are modeled as having a magnetic ordered core surrounded by a magnetically disordered shell whose thickness is estimated as about 1 nm.[22–26] These studies were performed in ferrimagnetic materials including $MnFe_2O_4$,[22] $CoFe_2O_4$,[23] and γ-Fe_2O_3,[24–26] and the techniques used have been magnetization,[22,25,26] Mössbauer spectroscopy,[25] and neutron diffraction.[23] In particular, the study of polarized neutron diffraction in surfactant coated and uncoated $CoFe_2O_4$ nanoparticles provided a better insight on the radial distribution of the magnetization.[23] The authors analyzed the XRD (400) reflection of this material to derive a crystalline particle size distribution and the same reflection in polarized neutron diffraction to extract the magnetically ordered size, smaller than the crystalline one, which corresponds to a magnetically dis-

 ©2010 The American Physical Society

ordered shell of about 1.2 and 1.7 nm thick.[23]

Here we report on the behavior of M_r induced by field cooling (fc) with different field intensities across T_N in CoO AF NPs of different sizes. The observed behavior is compared with that exhibit by a sample with bulk properties. Powder neutron-diffraction (PND) technique has been used as a function of temperature to investigate the relation between magnetic and structural parameters of the NP and the origin of the moments responsible for M_r.

II. EXPERIMENTAL

The CoO nanoparticles were prepared by adaptation of the method of Sun *et al.*[27] using cobalt acetate as the source of cobalt instead of cobalt formate. The size of the particles was adjusted by changing the cobalt to oleylamine ratio and the heating rate. In a typical synthesis, $Co(CO_2CH_3)_2$ was dispersed in oleylamine (in concentration ratios ranging from 1/12 to 1/48) and the mixture was heated at 100 °C for 30 min under N_2 atmosphere while repeatedly evacuated to remove oxygen and water. The solution was then heated up to 190 °C at different heating rates, from 10 to 20 °C/min, and kept for 3 h under vigorous magnetic stirring. After cooling the resulting solution to room temperature, the dark-brown suspension formed was precipitated by adding ethanol and repeatedly washed.

The sample with CoO nanoparticles with size $\langle\tau\rangle_{XRD}=24$ nm was prepared by a different method; the decomposition of cobalt cupferronate $[Co(cup)_2]$ in octadecene, accordingly to Ref. 28. Briefly, 0.25 g of $Co(cup)_2$ were added to 25 mL of octadecene and the mixture was sealed in a Teflon-lined stainless-steel autoclave. The autoclave was kept inside a preheated air oven at 250 °C for 48 h. After cooling to room temperature, the brownish-black solid was washed with toluene followed by methanol. The sample with CoO particles with larger size ($\langle\tau\rangle_{XRD}=190$ nm) is a comercial polycrystalline powdered sample obtained from Sigma-Aldrich.

Transmission electron microscopy (TEM) was performed using a Jeol-2000 FXII microscope, with point-to-point and line-to-line resolutions of 0.28 nm and 0.14 nm, respectively, and equipped with a INCA 200 X-Sight (Oxford Instruments) energy dispersive x-ray spectrometer (EDS). High-resolution TEM (HRTEM) images were obtained in a FEI TECNAI G2 F30 instrument. Samples for TEM observations were prepared by dispersing the nanoparticles in hexane and evaporating suspension drops on carbon-coated copper grids.

XRD measurements of CoO samples were performed at room temperature with a Philips X'Pert—MPD diffractometer using monochromated Cu $K\alpha$ radiation ($\lambda=1.541$ Å) in the 30°–80° 2θ range at 0.04° resolution and 4000 acquisition points per step. The incident-beam optics included a Soller slit of 0.04 rad, a 10 mm fixed mask, a divergence fixed slit of 0.5° and an antiscatter slit of 1°. The diffracted beam optics included a Soller slit of 0.04 rad and antiscatter slit of 6.6 mm. The analysis of the diffraction patterns was performed by Rietveld refinement using the FULLPROF package.[29] The size effects were treated with the integral breadth method using the Voigt model for both the instrumental and intrinsic diffraction peak shape considering a Thompson-Cox-Hastings pseudo-Voigt convoluted with axial divergence asymmetry function to describe the peak shape. The contribution of the instrument to the peaks broadening was determined by the refinement of the XRD pattern of a LaB_6 standard sample (NIST Ref. 660a). The contribution of the finite size of the nanoparticles crystallites to the peaks broadening was taken into account by an isotropic model yielding an apparent size, proportional to the mean size of the structurally ordered region of the nanoparticles $\langle\tau\rangle_{XRD}$.[29,30] In the following, samples will be identified by their $\langle\tau\rangle_{XRD}$ value.

PND was performed in the powder diffractometers D20 and D1A of the Institute Laue Langevin (ILL). At D20, the experiments were carried out using a monochromatic beam of 1.87 Å. Neutron diffractograms were recorded as a function of the temperature and magnetic field by means of introducing the sample in a standard vanadium can inside an ILL cryomagnet. Diffraction patterns from 2 to 297 K were collected at zero field, after zero-field cooling (zfc) and after fc the samples from 297 to 200 K under a magnetic field of 1×10^4 Oe applied perpendicular to the neutron beam. In order to have neutron data with less instrumental contribution to the peaks broadening and better accuracy in the determination of the nuclear and magnetic mean sizes, a PND pattern at 5 K was collected at the instrument D1A with a monochromatic beam of 1.90 Å. The analysis of the PND patterns was performed as described for the XRD patterns. The contribution of the instrument to the peaks broadening was determined by the instrument resolution function built from the refinement of a $Na_2Ca_3Al_2F_{14}$ standard sample while wavelengths were refined using a Si standard.

Magnetization was measured as a function of temperature from 2 to 300 K under a magnetic field of 100 Oe with a magnetic property measuring system (MPMS) model XL, Quantum Design Inc, equipped with a superconducting quantum interference device magnetometer. Two cooling procedures were used (i) zfc and (ii) field cooling across T_N, from 300 to 210 K and zfc from 210 to 2 K. The field cooling in the restricted temperature range near T_N of CoO was used to guarantee that only the moments associated to CoO are ordered in the presence of a field and not moments of a possible residual Co_3O_4 phase, which order at ~40 K. The remanent magnetization M_r was calculated from the difference between the magnetization obtained in (ii) and (i).

III. RESULTS AND DISCUSSION

A. Magnetic and nuclear structure

Rietveld analysis to XRD patterns [Fig. 1(a)] confirms the existence of CoO nanoparticles with mean structural coherence size $\langle\tau\rangle_{XRD}$ ranging from 18 to 68 nm. Sample from Sigma-Aldrich has a $\langle\tau\rangle_{XRD}=190$ nm. Any possible amount of Co_3O_4 present in the samples is below the detection limits.

TEM images of the sample with smaller nanoparticles ($\langle\tau\rangle_{XRD}=18$ nm) show that the CoO samples are composed of rhomboidal shaped nanoparticles with sizes on the order of 10 to 20 nm and some aggregates of these nanoparticles

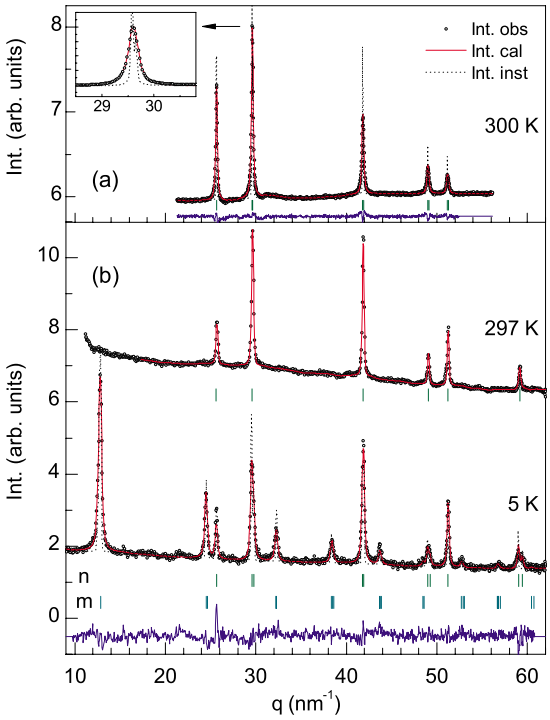

FIG. 1. (Color online) (a) XRD pattern of the CoO nanoparticles (sample with $\langle\tau\rangle_{XRD}=33$ nm) at 300 K. Vertical lines represent the position of the allowed Bragg peaks. Inset shows a zoom over the most intense peak. (b) PND pattern of the CoO nanoparticles (sample with $\langle\tau\rangle_{XRD}=40$ nm) at 297 K and at 5 K (instrument D20 and D1A, respectively). Vertical lines represent the position of the allowed Bragg peaks of nuclear (n) and magnetic (m) origin. In both panels, the instrument contribution to the peaks shape is shown in dotted lines and Rietveld refinement considering the finite-size effect of the nanoparticles to the peaks shape is shown in continuous (red) lines.

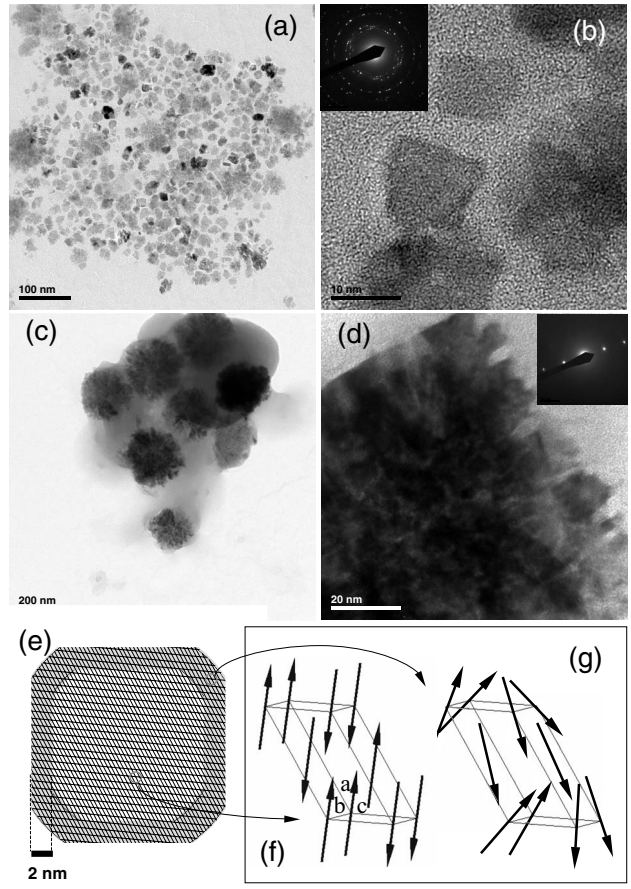

FIG. 2. (a) and (b) TEM images (scale bars correspond to 100 nm and 10 nm, respectively) of the CoO sample with $\langle\tau\rangle_{XRD}=18$ nm and inset showing an electron-diffraction image; [(c) and (d)] TEM images (scale bars correspond to 200 nm and 20 nm, respectively) of the CoO sample with $\langle\tau\rangle_{XRD}=40$ nm and inset showing an electron-diffraction image with spots corresponding to (111) and (222) reflections; (e) schematic representation of a CoO crystallite with a magnetic disordered layer of 2 nm; (f) magnetic structure of the nanoparticles core; and (g) representation of the magnetic disordered surface layer.

[Figs. 2(a) and 2(b)]. Electron-diffraction patterns show rings and spots at the distances expected for CoO while EDS gives a molar proportion of Co and O of 1:1.15, consistent with a slightly oxidized CoO. The sample with $\langle\tau\rangle_{XRD}=40$ nm consists of rhomboidal shaped aggregates with sizes of the order of 100 nm [Fig. 2(c)]. These aggregates are composed of smaller crystallites oriented in well-defined directions as deduced from the well-defined spots of electron diffraction [Fig. 2(d)].

HRTEM images of sample $\langle\tau\rangle_{XRD}=18$ nm show that the nanoparticles are single domain with planar boundaries and planes ordered up to the surface within the precision of the surface determination, estimated to be better than 0.4 nm [Fig. 3(a)]. The Fourier transform of the HRTEM images confirm that the nanoparticles are single domain. As expected, different zone axis are observed depending on the orientation of the nanoparticle, including the $[\bar{2}11]$ axis shown in Fig. 3(b).

The PND patterns performed in samples with $\langle\tau\rangle_{XRD}=40$ and 68 nm at room temperature confirm the information given by XRD, showing the peaks of the cubic face-centered CoO (space group $Fm\bar{3}m$).[31] As temperature decreases bellow T_N (which is in the 250–290 K range and depends on the particles size as discussed in the following section) the nuclear peaks become broader due to a monoclinic distortion (space group $C2/m$),[32] and peaks associated to AF magnetic ordering appear. At 5 K, the PND pattern can be well fit by a monoclinic nuclear cell [Fig. 1(b)] with parameters given in Table I and by a propagation vector $\mathbf{k}=[1/2,1/2,1/2]$ associated to a cubic cell, in accordance with Ref. 32. With respect to the monoclinic cell, $\mathbf{k}$ splits into the four vectors $\mathbf{k}_1=[0,1,1/2]$, $\mathbf{k}_{2,3}=[1/2,\pm 1/2,0]$,[32] and $\mathbf{k}_4=[0,0,1/2]$. Best fits are obtained with $\mathbf{k}_1$ and $\mathbf{k}_4$, with the moments aligned in the ac plane and making and angle φ with the a direction in the 45°–58° range and of about 18°, for $\mathbf{k}_1$ and $\mathbf{k}_4$, respectively. The magnetic structure corresponding to $\mathbf{k}_1$ is represented in Fig. 2(f). The solution with $\mathbf{k}_1$ is similar to that of Ref. 32, where the moments were found aligned in the ac plane with $\varphi=55°$. The values of φ for both $\mathbf{k}_1$ and $\mathbf{k}_4$ correspond to an angle ϕ between the moments and the plane defined by the ferromagnetically aligned moments [the (111) plane in the cubic cell] of about 12° and 18°, which are

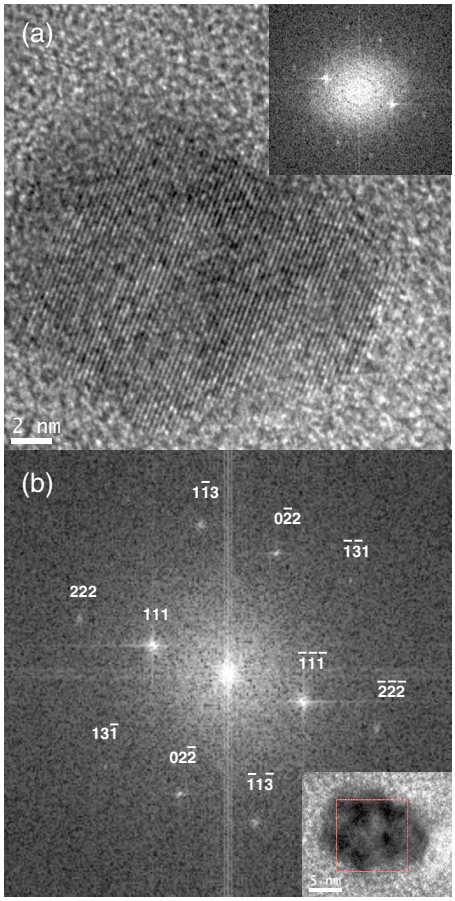

FIG. 3. (Color online) (a) HRTEM image of the CoO sample with $\langle\tau\rangle_{\mathrm{XRD}}=18$ nm and inset showing the Fourier transform of the image; and (b) Fourier transform of the rectangular region of the image show inset.

higher than the 8° found in Ref. 33 and the 1° and 4° recently found in Ref. 34. In fact, the magnetic structure of CoO is still a matter of debate, particularly in what concerns to the existence of single or multi-**k** structures[35] and the moments direction. The present results show that the magnetic structure of the CoO nanoparticles is compatible to that found for bulk powder and single-crystal CoO.

The magnetic moment per Co ion at 5 K for $\mathbf{k}_1$ in samples with $\langle\tau\rangle_{\mathrm{XRD}}=40$ and 68 nm is 3.41(7) and 3.40(4) μ_B, respectively (Table I); similar values are obtained for $\mathbf{k}_4$. These values are close to those reported in Ref. 36 (3.4 ± 0.1 μ_B) and slightly smaller than that reported in Ref. 32 [3.98(6) μ_B] and Ref. 37 (3.8 μ_B). All these values are higher than the spin-only moment of 3 μ_B, indicating an important orbital contribution.

As temperature increases, the magnetic (sublattice) moment M_{sub} of samples $\langle\tau\rangle_{\mathrm{XRD}}=40$ and 68 nm decreases, similarly to that reported for bulk.[36] At lower temperatures ($T/T_N<0.5$), $M_{sub}(T)$ in the bulk was described by spin waves while close to T_N it follows a Brillouin law. At intermediate temperatures non of these models apply [see Fig. 7(b) for comparison between $M_{sub}(T)$ and Brillouin law in sample with $\langle\tau\rangle_{\mathrm{XRD}}=68$ nm].

In both samples, the mean size of the structurally ordered region obtained from the XRD patterns is higher than that obtained from the PND data (Table I). This might be due to uncertain associated to the determination of the instrument resolution function. At the same time, the nuclear (structural) coherence size of both samples is higher than the magnetic coherence size. In the sample with smaller size, where the contribution to the PND peaks broadening due to the sample is more relevant and thus the accuracy in the sizes determination is better, the difference between the structural and magnetic sizes is consistent in the two instruments used (5.4 nm and 4.4 nm in D20 and D1A, respectively). Considering the value obtained in the instrument with better resolution in the low angle region (D1A), the CoO nanoparticles of sample $\langle\tau\rangle_{\mathrm{XRD}}=40$ nm can be described by a core-shell model, where the core is structural and magnetically ordered and the shell is structurally ordered and magnetically disordered, with a thickness of about 2 nm, corresponding to about seven nuclear cells in the c direction, as depicted in Fig. 2(e).

B. Size dependence of T_N

At temperatures in the 240–290 K range, the magnetic susceptibility has a maximum. In the context of magnetic nanoparticles, this could correspond to a T_N or to a blocking temperature T_B. The former is associated to the intraparticle AF ordering. The latter is associated to the temperature below which the magnetic moment of the nanoparticles is not

TABLE I. Nuclear and magnetic parameters (propagation vector $\mathbf{k}_1=[0,1,1/2]$) obtained from Rietveld refinement of neutron-diffraction data. Numbers in parenthesis denote the standard deviation expressed in units of the least significant digit. The standard deviation of the size was estimated based on the standard deviation of the fitted parameters and disregarding the uncertain associated to the determination of the parameters associated to the instrument contribution.

		Nuclear							Magnetic			
$\langle\tau\rangle_{\mathrm{XRD}}$ (nm)	Instrument	T (K)	a (Å)	b (Å)	c (Å)	β (deg)	Size (nm)	Bragg-R	μ (μ_B)	φ (deg)	Size (nm)	Mag-R
40	D20	2.1	5.178(1)	3.0066(5)	3.0051(5)	125.49(2)	30.8(2)	4.84	3.41(7)	50(1)	25.4(3)	12.4
	D1A	5.4	5.1895(6)	3.0106(5)	3.0116(5)	125.464(9)	24.1(2)	4.25	3.44(7)	59(1)	19.7(2)	5.83
	D20	295	4.2476(6)					6.86				
68	D20	5.4	5.1828(6)	3.0123(3)	3.0110(3)	125.512(8)	57(1)	9.43	3.40(4)	44.9(7)	40(1)	16.9
	D20	305	4.2558(1)					3.38				

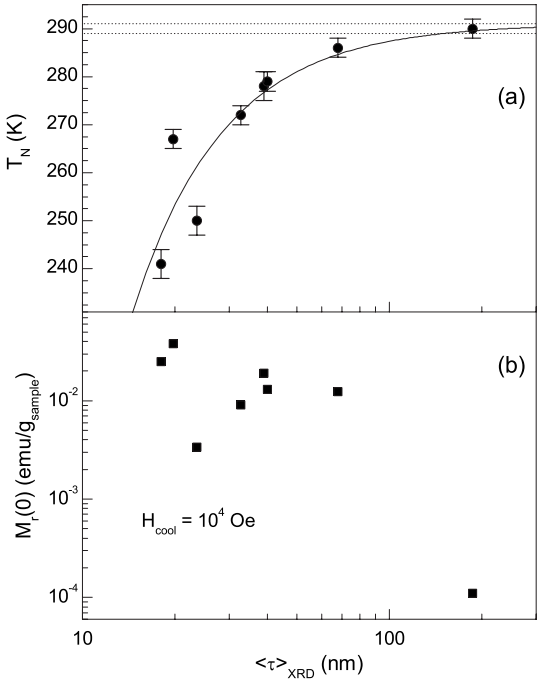

FIG. 4. (a) Dependence of the Néel temperature T_N (determined from magnetic-susceptibility data) with the structural mean size $\langle\tau\rangle_{\mathrm{XRD}}$ (determined from Rietveld refinement to XRD data). Horizontal dotted lines delimitate the range of values for T_N in bulk samples. Continuous line represents the fit to Eq. (1). (b) Dependence of the remanent magnetization at zero temperature $M_r(0)$ (obtained after cooling the samples with a field of 1×10^4 Oe) with $\langle\tau\rangle_{\mathrm{XRD}}$ in a log-log plot.

able to cross the anisotropy energy barrier within the experimental characteristic time, being a dynamical phenomena always associated to a frequency-dependent ac susceptibility and to the existence of an out-of-phase component.[38] Since the PND measurements (which are directly probing the phase transition via the ordering parameter) performed in samples with $\langle\tau\rangle_{\mathrm{XRD}}$=40 and 68 nm yield T_N values at the temperatures where the susceptibility peaks occur and since no frequency dependence or out-of-phase susceptibility is found in the 240–320 K range, the peaks of the magnetic susceptibility are associated with T_N. In fact, it is expected that within the characteristic sizes here studied (>18 nm) T_N estimated from susceptibility peaks approaches the true thermodynamic values, in accordance to that shown for CoO films, where for thicknesses higher than ~4 nm T_N estimated from susceptibility peaks approaches the true values measured by heat capacity.[39]

As the size of the nanoparticles decreases, the transition temperature T_N (estimated from the maximum of the zfc susceptibility curve) decreases [Fig. 4(a)]. This decrease can be described in first approach by the finite-size scaling dependence

$$\frac{T_N(\infty)-T_N(D)}{T_N(\infty)}=\left(\frac{\varepsilon_0}{\langle\tau\rangle_{\mathrm{XRD}}}\right), \qquad (1)$$

where ε_0 is the correlation length at T=0 and λ_d is the shift exponent for the finite-size scaling.[40] By fixing $T_N(\infty)$ within the limits found in literature,[36,37] the best fit is obtained with ε_0=5 nm and λ_d=1.5. ε_0 is larger than the value found in CoO films (1.8 nm) while the value of λ_d is similar (λ_d=1.55), being between the value corresponding to those of Ising (λ_d=1.56) and three-dimensional Heisenberg systems (λ_d=1.42).[41]

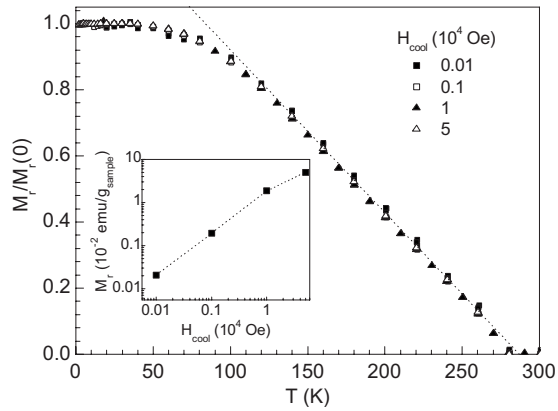

FIG. 5. Temperature dependence of the reduced remanent magnetization $M_r/M_r(0)$ of sample with $\langle\tau\rangle_{\mathrm{XRD}}$=39 nm obtained for different cooling fields H_{cool}. Inset shows the dependence of M_r at 2 K with H_{cool}.

These $T_N(\langle\tau\rangle_{\mathrm{XRD}})$ results demonstrate that in the CoO NP, finite-size effects are relevant and contribute to the reduction in T_N, despite their aggregation state. We notice that T_N may also be affected by the magnetically disordered layer identified by PND, although the present results are inconclusive on this respect. In the CoO sample from Sigma-Aldrich T_N is within the values found in bulk samples,[36,37] and therefore finite-size effects are not relevant. In the view of finite-size effects, this sample can be used as a reference for CoO bulk magnetic behavior.

C. Remanent magnetization

The remanent magnetization induced by cooling in the presence of a magnetic field, determined as described in Sec. II, saturates at low temperature and decreases almost linearly with the temperature up to temperatures near T_N (Fig. 5). As the cooling field H_{cool} increases, M_r at 2 K also increases, following a power law with an exponent close to 1, in first approach and within the studied field range (Fig. 5, inset). This contrasts with the H^2 dependence of M_r with origin in domain walls of bulk AF materials.[1] On the other hand, M_r is still not saturated at fields much higher than those typical of AF materials with diluted impurities.[2]

The reduced remanent magnetization of the CoO NP $M_r/M_r(0)$ (with $M_r(0)$ taken as the value at 2 K) scales with H_{cool}, as represented in Fig. 5 for sample with $\langle\tau\rangle_{\mathrm{XRD}}$ =39 nm, showing that as H_{cool} increases a larger net moment is being kept in the field direction while having similar origin/mechanism.

The dependence of $M_r(0)$ with size is scattered [Fig. 4(b)]. However, it is clear that in the nanoparticles $M_r(0)$ is enhanced compared to bulk and in the nanoparticles where $\langle\tau\rangle_{\mathrm{XRD}}$ is about one order of magnitude lower than that of

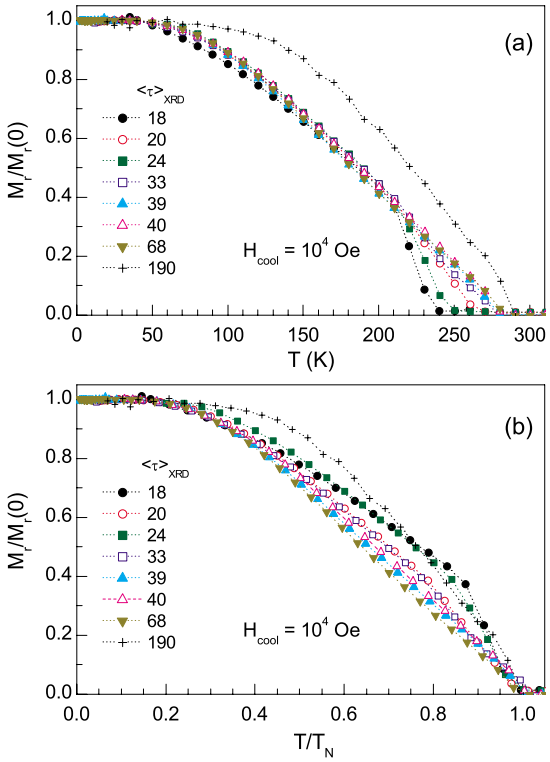

FIG. 6. (Color online) (a) Temperature dependence of the reduced remanent magnetization $M_r/M_r(0)$ of all studied samples obtained after cooling under $H_{cool}=1\times10^4$ Oe. (b) $M_r/M_r(0)$ of all studied samples obtained after cooling under $H_{cool}=1\times10^4$ Oe as a function of the reduced temperature T/T_N.

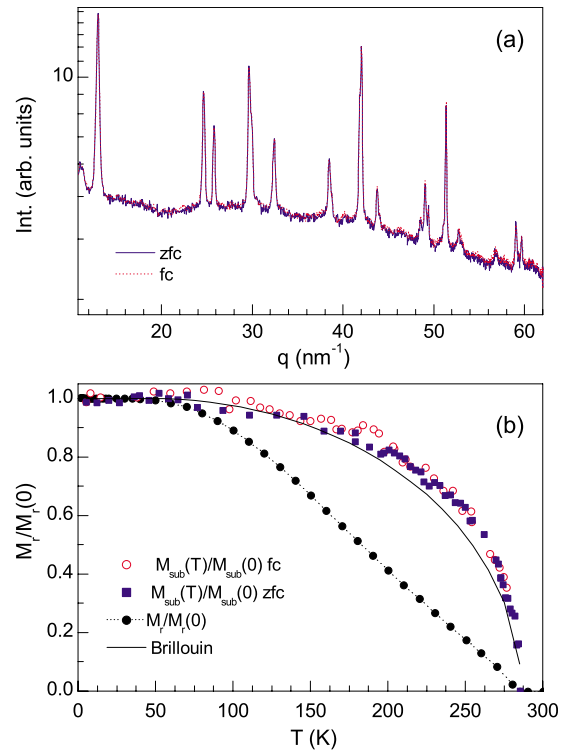

FIG. 7. (Color online) (a) PND pattern of the CoO nanoparticles (sample with $\langle\tau\rangle_{XRD}=68$ nm) at 5 K after zfc and fc (instrument D20). (b) Temperature dependence of the reduced remanent magnetization $M_r/M_r(0)$ of sample with $\langle\tau\rangle_{XRD}=68$ nm compared to the reduced sublattice magnetization $M_{sub}/M_{sub}(0)$ obtained from Rietveld refinement to zfc and fc PND patterns. Continuous line represents the Brillouin law for $T_N=286$ K and $S=3/2$.

bulk, $M_r(0)$ is about two orders of magnitude higher.

Comparing $M_r/M_r(0)$ for the different studied sizes [Fig. 6(a)], it is interesting to note that it scales for the samples containing nanoparticles in the low and medium temperature range (in the saturation and linear region), separating only near T_N since the samples have different T_N values. This scaling is far better than the scaling in a $M_r/M_r(0)$ vs T/T_N scale [Fig. 6(b)]. In fact, in all samples the linear region of $M_r/M_r(0)$ extrapolates to zero remanent magnetization for temperatures near to the bulk T_N. At low/medium temperatures, the remanent moments behave as there was no reduction in T_N due to size effects; in other words, finite-size effects are relevant only near T_N.

$M_r/M_r(0)$ of the sample taken as bulk does not scale in T nor T/T_N, showing that in this sample M_r has a different origin, probably domain walls, as usually found in bulk AF.[1] Also, the temperature dependence of M_r is different from that arising from interfacial uncompensated moments in CoO films, where a plateau up to 200 K was found.[4]

In order to have a better insight on the origin of the moments associated to the M_r induced by H_{cool} we have performed PND experiments as a function of temperature at zero field, after zfc and after field cooling across T_N, in samples $\langle\tau\rangle_{XRD}=40$ and 68 nm. It is clear that PND patterns taken after zfc and fc are equal, within the experimental precision [Fig. 7(a)]. Since the integral breadth of the magnetic peaks remains unchanged by fc, the size of the magnetically ordered core also remains unchanged, within the precision of a few standard deviations (see standard deviations in Table I). In this view, M_r arises most probably from magnetic moments located at the magnetically disordered surface and not from an important change in the size of the magnetically ordered core induced by fc. The surface origin of M_r is also supported by the linear behavior of $M_r(T)$ at intermediate temperatures. In fact, the linear $M_r(T)$ indicates that the moments responsible for the remanent magnetization are in a two-dimensional (2D) configuration as experimentally[42,43] and theoretically[44] found in films and particles.[19,45] Furthermore, Makhlouf *et al.*[16] refer to molecular-field calculations showing that the linearity holds down to $T/T_N=0.2$, similarly to that found here [Fig. 6(b)].

From the point of view of the $M_r(T)$ dependence, it is expected that a 2 nm thick shell behaves as a 2D entity based on models and experimental results. Models show that $M(T)$ depends on the number of atomic layers n, on the spin value and on the ratio between the parallel magnetic anisotropy constant and the exchange constant.[44] For some typical values of this ratio, it is shown that for $n>10$, $M(T)$ become similar to bulk. In the present case of CoO, 2 nm correspond to about 7 Co layers, which is within the range where a shell is expected to behave as a 2D entity. An experimental study in $La_{0.7}Sr_{0.3}MnO_3$ films[43] show that $M(T)$ probed in a 5 nm thick surface is still substantially different from that of bulk and conclude that at least several monolayers below a 0.5 nm surface boundary $M(T)$ is considerably different from bulk.

IV. CONCLUSIONS

In this paper we show that a remanent moment M_r can be induced in CoO nanoparticles by crossing the transition temperature in the presence of a magnetic field, with M_r being approximately proportional to the cooling field. The value of M_r at low temperature in the nanoparticles is about two orders of magnitude higher than the value found in the sample taken as the bulk. The nanoparticles are well described by a core-shell model with the following characteristics (i) the core is magnetically similar to that of the bulk (concerning both the value and direction of the magnetic moment), (ii) the core remains unchanged by cooling across T_N in the presence of a magnetic field compared to the zero-field cooling situation within the instrumental precision, (iii) both core and shell are structurally ordered, (iv) the shell is structurally ordered and magnetically disordered having a thickness of about 2 nm, and (v) most probably M_r arises from pinned uncompensated/canted moments located at the shell. Points (iii) and (iv) are supported by PND and point (iii) is also in accordance with HRTEM images which show that the nanoparticles are single domain and the crystalline planes are ordered across the nanoparticles up to near the surface. Point (v) is supported by the linear dependence of M_r with temperature. The existence of a structurally ordered and magnetically disordered shell opens the question of the source of this magnetic disorder. This source can be structural, including preferential surface vacancies (which lead to broken exchange paths and oxidized nonmagnetic Co) and surface tension. Magnetic sources include an odd number of planes and the symmetry break of the exchange paths of surface atoms. The latter gives rise to a progressively canting of the moments.[46] Another magnetic source for the generation of a pinned moment was discussed for NiO.[17] Accordingly to numerical modeling, the reduced coordination of surface spins leads to different sublattice configurations, which causes changes in the magnetic order throughout the particle. This last cause is clearly compatible with the present experimental findings.

ACKNOWLEDGMENTS

We acknowledge the collaboration of Thomas Hansen in the experiments at D20 and ILL for beamtime allocation. We also acknowledge R. Soares for the XRD patterns and A. Ferreira for enlightening comments about XRD instrumental contribution. The Aveiro-Zaragoza collaboration has been supported by the Integrated Spanish-Portuguese Action under Grant No. PT2009-0131. The work in Zaragoza has been supported by the research Grants No. MAT2007-61621, No. MAT2009-13977-C03-01, and No. CONSOLIDER CSD2007-00010 from the Ministry of Education. N.J.O.S. acknowledges CSIC for a I3P contract and FCT for Ciencia 2008 program.

*Present address: CICECO, Universidade de Aveiro, 3810-193 Aveiro, Portugal; nunojoao@ua.pt

[1] P. Pollak, W. Kleemann, and D. P. Belanger, Phys. Rev. B **38**, 4773 (1988).
[2] F. Palacio, M. Gabás, J. Campo, C. C. Becerra, A. Paduan-Filho, and V. B. Barbeta, Phys. Rev. B **56**, 3196 (1997).
[3] Ò. Iglesias, A. Labarta, and X. Batlle, J. Nanosci. Nanotechnol. **8**, 2761 (2008).
[4] K. Takano, R. H. Kodama, A. E. Berkowitz, W. Cao, and G. Thomas, Phys. Rev. Lett. **79**, 1130 (1997).
[5] A. E. Berkowitz, G. F. Rodriguez, J. I. Hong, K. An, T. Hyeon, N. Agarwal, D. J. Smith, and E. E. Fullerton, Phys. Rev. B **77**, 024403 (2008).
[6] W. H. Meiklejohn and C. P. Bean, Phys. Rev. **105**, 904 (1957).
[7] V. Skumryev, S. Stoyanov, Y. Zhang, G. Hadjipanayis, D. Givord, and J. Nogués, Nature (London) **423**, 850 (2003).
[8] I. V. Golosovsky, G. Salazar-Alvarez, A. López-Ortega, M. A. González, J. Sort, M. Estrader, S. Suriñach, M. D. Baró, and J. Nogués, Phys. Rev. Lett. **102**, 247201 (2009).
[9] A. H. Morrish and K. Haneda, J. Magn. Magn. Mater. **35**, 105 (1983).
[10] T. Okada, H. Sekizawa, F. Ambe, S. Ambe, and T. Yamadaya, J. Magn. Magn. Mater. **31-34**, 903 (1983).
[11] F. T. Parker and A. E. Berkowitz, Phys. Rev. B **44**, 7437 (1991).
[12] F. T. Parker, M. W. Foster, D. T. Margulies, and A. E. Berkowitz, Phys. Rev. B **47**, 7885 (1993).
[13] A. E. Berkowitz, J. A. Lahut, and C. E. Van Buren, IEEE Trans. Magn. **16**, 184 (1980).
[14] P. Guardia, B. Batlle-Brugal, A. G. Roca, Ò. Iglesias, M. P. Morales, C. J. Serna, A. Labarta, and X. Batlle, J. Magn. Magn. Mater. **316**, e756 (2007).
[15] M. M. Ibrahim, J. Zhao, and M. S. Seehra, J. Mater. Res. **7**, 1856 (1992).
[16] S. A. Makhlouf, F. T. Parker, and A. E. Berkowitz, Phys. Rev. B **55**, R14717 (1997).
[17] R. H. Kodama and A. E. Berkowitz, Phys. Rev. B **59**, 6321 (1999).
[18] A. Punnoose, H. Magnone, M. S. Seehra, and J. Bonevich, Phys. Rev. B **64**, 174420 (2001).
[19] D. L. Mills, Phys. Rev. B **3**, 3887 (1971).
[20] A. H. Morrish and K. Haneda, J. Appl. Phys. **52**, 2496 (1981).
[21] K. Haneda and A. H. Morrish, J. Appl. Phys. **63**, 4258 (1988).
[22] Z. X. Tang, C. M. Sorensen, K. J. Klabunde, and G. C. Hadjipanayis, Phys. Rev. Lett. **67**, 3602 (1991).
[23] D. Lin, A. C. Nunes, C. F. Majkrzak, and A. E. Berkowitz, J. Magn. Magn. Mater. **145**, 343 (1995).
[24] B. Martínez, X. Obradors, Ll. Balcells, A. Rouanet, and C. Monty, Phys. Rev. Lett. **80**, 181 (1998).
[25] S. Linderoth, P. V. Hendriksen, F. Bødker, S. Wells, K. Davies, S. W. Charles, and S. Mørup, J. Appl. Phys. **75**, 6583 (1994).
[26] A. Millan, A. Urtizberea, F. Palacio, N. J. O. Silva, V. S. Amaral, E. Snoeck, and V. Serin, J. Magn. Magn. Mater. **312**, L5 (2007).
[27] X. Sun, Y.-W. Zhang, R. Si, and C.-H. Yan, Small **1**, 1081 (2005).
[28] M. Ghosh, E. V. Sampathkumaran, and C. N. R. Rao, Chem. Mater. **17**, 2348 (2005).

[29] J. Rodríguez-Carvajal, Physica B **192**, 55 (1993).
[30] D. Martínez-Blanco, P. Gorria, J. A. Blanco, M. J. Pérez, and J. Campo, J. Phys.: Condens. Matter **20**, 335213 (2008).
[31] J. D. Hanawalt, H. W. Rinn, and L. K. Frevel, Ind. Eng. Chem. Anal. Ed. **10**, 457 (1938).
[32] W. Jauch, M. Reehuis, H. J. Bleif, F. Kubanek, and P. Pattison, Phys. Rev. B **64**, 052102 (2001).
[33] D. Herrmann-Ronzaud, P. Burlet, and J. Rossat-Mignod, J. Phys. C **11**, 2123 (1978).
[34] E. Ressouche, N. Kernavanois, L.-P. Regnault, and J.-Y. Henry, Physica B **385-386**, 394 (2006).
[35] K. Tomiyasu, T. Inami, and N. Ikeda, Phys. Rev. B **70**, 184411 (2004).
[36] M. D. Rechtin and B. L. Averbach, Phys. Rev. B **6**, 4294 (1972).
[37] W. L. Roth, Phys. Rev. **110**, 1333 (1958).
[38] J. L. Dormann, D. Fiorani, and E. Tronc, *Advances in Chemical Physics* (Wiley, New York, 1997), Vol. 98.
[39] Y. J. Tang, D. J. Smith, B. L. Zink, F. Hellman, and A. E. Berkowitz, Phys. Rev. B **67**, 054408 (2003).
[40] M. E. Fisher and M. N. Barber, Phys. Rev. Lett. **28**, 1516 (1972).
[41] T. Ambrose and C. L. Chien, Phys. Rev. Lett. **76**, 1743 (1996).
[42] G. Xiao, C. L. Chien, and M. Natan, J. Appl. Phys. **61**, 4314 (1987).
[43] J.-H. Park, E. Vescovo, H.-J. Kim, C. Kwon, R. Ramesh, and T. Venkatesan, Phys. Rev. Lett. **81**, 1953 (1998).
[44] A. Corciovei, Phys. Rev. **130**, 2223 (1963).
[45] Ò. Iglesias and A. Labarta, Phys. Rev. B **63**, 184416 (2001).
[46] L. Néel, J. Phys. Soc. Jpn. **17**, Suppl. B, 676 (1962).